Biomass Conversion and Biorefinery (2025) 15:2285–2302
https://doi.org/10.1007/s13399-023-04954-8

ORIGINAL ARTICLE

Endophytic fungi–assisted biomass synthesis of gold, and zinc oxide nanoparticles for increasing antibacterial, and anticancer activities

Sameh E. Hammad[1] · Mahmoud N. El-Rouby[2] · Marwa M. Abdel-Aziz[3] · Gharieb S. El-Sayyad[4,5,6] · Hussein H. Elshikh[1]

Received: 24 July 2023 / Revised: 25 September 2023 / Accepted: 26 September 2023 / Published online: 16 October 2023
© The Author(s) 2023

Abstract

Pathogenic microorganisms and cancer continue to be the most difficult problem in public health care and the incidence of diseases caused by such resistant strains and cancer cells are growing. Recent advances in nanotechnology open up new possibilities for creating novel, exciting nanoparticles that are safe for human cells and may be used as smart antibacterial and anticancer medicines. The novelty of the present study is the extracellular green synthesis of zinc oxide nanoparticles (ZnO NPs), and gold (Au) NPs using the cell filtrate of the endophytic fungus *Fusarium chlamydosporum* MW341592.1 isolated from healthy leaves of *Eucalyptus sideroxylon* plant. Eco-friendly synthesized ZnO NPs and Au NPs were screening for their activity against select carcinomic cell lines and some multidrug-resistant bacteria. The synthesized ZnO NPs and Au NPs were characterized by UV-Vis. spectroscopy, X-ray diffraction (XRD), dynamic light scattering (DLS), transition electron microscopy (TEM), and energy-dispersive X-ray spectroscopy (EDX). The UV-Vis. absorption spectra of the produced ZnO NPs showed bands in the UV area at 320 nm, whereas the Au NPs showed bands in the UV region at 530 nm. TEM revealed average sizes for ZnO NPs, and Au NPs as 19.3 nm and 22.1 nm, respectively, while shape revealed both ZnO NPs and Au NPs with spherical-like shape. Biological assay showed that raising in the synthesized NP concentration lowers the number of HCT-116 human colon cancer cells and CACO2 human intestinal cancer cells, as well as associated pathogens such as *Escherichia coli* and *Pseudomonas aeruginosa.*

Keywords Endophytic fungi · Zinc oxide nanoparticles · Antibacterial activity · Anticancer potential · Gold nanoparticles

1 Introduction

According to a WHO and NCI estimate, cancer represents one of the top causes of death and a major impediment to increasing life expectancy, accounting for ten million deaths in 2020. By 2040, the number of newly diagnosed cancer cases is estimated to rise to 29.5 million each year, with cancer-related fatalities rising to 16.4 million per year [1, 2]. Traditional cancer therapies include chemotherapy and radiation, but all of these methods have substantial side effects due to their inability to differentiate malignant cells from healthy cells. Considering this, most patients are treated with a combination of surgical surgery, radiation, and chemotherapy. Because of the toxicity of anticancer drugs, poor selectivity, the potential of cancer recurrence, and the development of drug-resistant cancer cells, the use of these treatments is limited [3]. As a result, there is a growing demand for the discovery and identification of novel medications as anticancer treatment

✉ Gharieb S. El-Sayyad
Gharieb.Elsayyad@gu.edu.eg

1 Botany and Microbiology Department, Faculty of Science, Al-Azhar University, Nasr City, Cairo 11884, Egypt

2 Cancer Biology Department, Egyptian National Cancer Institute, Cairo University, Cairo, Egypt

3 Regional Center of Mycology and Biotechnology, Al-Azhar University, Nasr City, Cairo 11884, Egypt

4 Department of Microbiology and Immunology, Faculty of Pharmacy, Ahram Canadian University, Sixth of October City, Giza, Egypt

5 Department of Microbiology and Immunology, Faculty of Pharmacy, Galala University, New Galala city, Suez, Egypt

6 Drug Microbiology Lab., Drug Radiation Research Department, National Center for Radiation Research and Technology (NCRRT), Egyptian Atomic Energy Authority (EAEA), Cairo, Egypt

with minimal side effects as confirmed by nanotechnology approach, such as the use of ZnO NPs [4, 5].

Colorectal and esophageal cancers are the fourth and eighth most frequent malignancies worldwide, respectively [6]. Colon cancer is a fatal malignant cancer with an increased incidence rate in those aged 40 to 50, and it is a leading cause of mortality. Every year, it accounts for 1.36 million new cases and 774,000 mortality worldwide [7].

Furthermore, a microbial infection causes almost 20% of all malignancies [8]. According to Safdar and Armstrong [9], bacteraemia is a major source of life-threatening complications in cancer patients, particularly those who take anti-cancer treatment. Because of inflammatory sores on mucosal surfaces and immune suppression caused by chemotherapy, cancer patients are more prone to invasive infection [9]. Many studies link Gram-negative bacteria to bloodstream infections in cancer patients [10]. *Pseudomonas aeruginosa* colonizes the human gut frequently during hospitalization, immunosuppression, antibiotic therapy, surgery, severe trauma, and other situations that cancer patients may confront [11]. *P. aeruginosa* has long been recognized as one of the leading causes of severe sepsis and mortality in people with cancer having neutropenia [12]. Patel et al. [13] identified colon cancer and shed light on the infectious proclivity of *E. coli* bacteremia to the development of colon adenocarcinoma [13]. According to Marco et al. [14], some *E. coli* strains that produce the genotoxin colibactin have been linked to the development and progression of colon cancer [14]. Buc et al. discovered cyclomodulin synthesis by *E. coli* from phylogenetic group B2 in biopsies from colon cancer patients, as well as pathways implicated in cancer formation [15].

MDR microorganisms continue to be the most difficult problem in public health care. Globally, the incidence of diseases caused by such resistant strains is growing. Pathogen-acquired resistance is a significant concern for many antimicrobial medicines. Recent breakthroughs in nanotechnology provide new perspectives for developing unique formulations based on diverse types of NPs with varying sizes and shapes, as well as flexible antibacterial capabilities [16].

During the previous decade, nanotechnology has emerged as a technology that has altered every field of applied science. The field of NPs, which is associated with nanostructured materials with very small particle sizes varying from 1 to 100 nm, is one of the approaches to nanotechnology [17]. Because of their small size and high surface area-to-volume ratio, NPs have distinct characteristics than their bulk counterparts, resulting in significant differences in features [18]. Nanotechnology research has recently become a priority topic at the forefront of contemporary research in a variety of domains such as medicine, physics, chemistry, biology, and so on [19, 20].

Nanomedicine is the use of nanotechnology to treat, diagnose, monitor, and control illnesses. Despite recent medical improvements, several disorders, including AIDS [21], tumor [22], bacterial infections [23], diabetes [24], chronic pain [25], and autoimmune disorders [26], remain untreated. Because nanoparticles are the cornerstone of nanotechnology, their use in medicine has opened up new avenues for treatment [27].

Chemical and physical methods for NP synthesis have become popular in recent years due to the use of less energy during metal reduction and the formation of homogenous NPs with high accuracy [28]. Thus, typical NP synthesis methods are arduous, time-consuming, dangerous, and rely on the use of toxic compounds that are unhealthy (cytotoxic, genotoxic, carcinogenic) and function as potent environmental pollutants [29]. Furthermore, due to their instability and toxicity, the biological uses of NPs derived through chemosynthesis have been limited [30]. As a result, there is a difficult scientific necessity to identify alternate green sources to address these disadvantages. The hardest job in green synthesis of metal nanoparticles is to identify an appropriate and nontoxic natural product, as well as an eco-friendly solvent solution [31].

Green synthesis employing plant extracts or microorganisms is a clean method since no hazardous chemicals are used in the production process; also, the synthesis process happens under moderate pressure and temperature conditions and at a lower cost [32, 33]. Using many sorts of biological systems, eco-friendly and low-cost methods might be developed. These are referred to as "biological techniques of synthesis," and they involve bacteria, fungi, yeasts, microalgae, macro algae, and plant extracts [34].

Endophytes are fungal or bacterial members that live inside plant tissues for brief periods of time or throughout the plant's life cycle without negatively affecting the host plant [35]. *E. robusta* possesses pharmacological efficacy, particularly in cancer and inflammation, as well as antioxidant and antibacterial properties [36].

Various chemical and physical methods are used to create ZnO NPs. Nonetheless, these methods are costly and harmful to the environment. As a result, the biosynthesis of ZnO NPs has lately advanced fast, with microorganisms that are cleaner, eco-friendly, non-toxic, and biocompatible as alternatives to chemical and physical methods [18]. Because of its biodegradability, low toxicity, and low cost, ZnO NP has been employed in an increasing variety of commercial goods such as paint, coating, cosmetics, and biomedicine [37] during the last two decades, notably in the anticancer or antibacterial domains [38].

ZnO NP are antimicrobial and inhibit microbe formation by entering the cell membrane. In *E. coli*, it has been supported by an oxidative stress mechanism involving zinc oxide nanoparticles [39]. Their low toxicity to human cells,

low cost, size-dependent effective inhibition against a wide range of bacteria, capacity to prevent biofilm development, and even elimination of spores make them appropriate for use as anti-bacterial agents in fabrics [40]. Interestingly, multiple investigations have found that ZnO NPs are non-toxic to human cells [41, 42], which has required their use as antibacterial agents, hostile to microorganisms, and have high biocompatibility with human cells [43].

Antibiotic abuse has resulted in an increase in bacterial resistance and, as a result, a decrease in the efficacy of the few available antibiotics. Alternatively, due to their large specific surface area, ease of modification by functional groups, and broad-spectrum antibacterial action, Au NPs are potential antibacterial behavior. Their antibacterial effects are directly connected to particle size, dispersibility, and surface modification, all of which may be modified by varying reaction conditions [44].

Nanomaterials are predicted to change cancer detection and treatment [45]; colorectal cancer (CRC) is the second fatal cancer and the third most common malignant tumor. There had been 1.8 million new CRC cases in 2018, with approximately 900,000 deaths [46]. By 2035, the number of new cases is predicted to reach approximately 2.5 million [47]. The synthesized NPs demonstrated anticancer efficacy in the treated HepG2 liver cancer cell line, as well as a noteworthy non-toxic impact on the normal VERO cell line [48]. Previous study discovered that Au NPs had good anticancer capabilities against a range of cell lines, including ADR/MCF-7 cancer cells, Lewis lung carcinoma (LL2) cells, HCT15, HCT116, HT29, A549 lung epithelial cancer cell line, and RKO colon cancer cell lines, LN229 human glioma cancer lines, A549 cells, U87, HDF, HeLa cells, HepG2, and C0045C, 4T [49, 50].

This study aims to biosynthesize and characterize ZnO NPs, and Au NPs using the extract of endophytes *F. chlamydosporum* isolated from the leaves of *E. sideroxylon* plant for the first time, and additionally, to assess their antimicrobial, as well as anticancer activities for possible application in biomedical fields as safe and an ecofriendly catalytic agents.

2 Materials and methods

2.1 Chemicals and materials

All of the chemicals and reagents utilized in this investigation were of analytical grade and were not purified further. NanoTech for Photo-Electronics, City of 6 October, Giza, Egypt, supplied anhydrous zinc sulfate (Zn SO_4) and gold chloride dihydride ($HAuCl_4 \cdot 2H_2O$). Crystal violet and dimethyl sulfoxide (DMSO) had been purchased from Sigma Aldrich, USA, and trypan blue dye from St. Louis, Mo., USA.

2.2 Cell lines

VACSERA for Biological Products and Vaccines SAE, Giza, Egypt, provided the HCT116 and CACO2 cell lines. All of the chemicals and microbiological medium used were of analytical quality and did not need to be purified further.

2.3 Microorganisms

In the extended-spectrum beta-lactamase according to the American Type Culture Collection, the *Escherichia coli* BAA-199 strain belongs to the SHV-3-ESBL class, which contains ESBL enzymes that confer resistance to extended-spectrum cephalosporins and monobactams.

Multiple drug resistance *Pseudomonas aeruginosa* BAA-2112 is a Gram-negative strain with resistance up to 15 antibiotics, including penicillins, cephalosporins, carbapenems, quinolones, and aminoglycosides, according to the American Type Culture Collection. They were graciously provided by the National Research Center in Giza, Egypt.

2.4 Plant

Healthy *Eucalyptus sideroxylon* plant samples were obtained from Desert Research Center, Egypt; to acquire endophytes, separate sterile polythene bags were utilized to transport healthy plant samples from their native habitat. According to Fisher and Petrini [51], the samples were transported into the laboratory and processed within 24 h [51].

2.5 Isolation of endophytic fungi

Healthy small cuttings of some *Eucalyptus sideroxylon* plant leaves were gathered. Entophytic fungi were isolated from plant parts using the technique described by Hallman et al. [52], with the following modifications: To eliminate dust and dirt, healthy leaves were carefully cleaned under running tap water. Explants were washed well before being sliced into 0.5 cm × 0.5–1 cm slices without the midrib under aseptic conditions.

Surface sterilization of explants was achieved by immersing them in 70% ethanol for 30 s, followed by 3 min in a 13% commercial bleach solution (Clorox) (sodium hypochlorite solution), followed by three rinses with sterile distilled water. Explants were placed on sterile Petri dishes with sterile potato dextrose agar (PDA) treated with chloramphenicol (50 mg/L) to limit bacterial proliferation. All dishes were covered with par film and cultured at 28°C for up to 7 days, following which emerging fungi were purified and

transferred to fresh sterile PDA plates for another 7 days of incubation [53].

2.6 Identification of fungal isolates

Using an image analysis approach, the most potent fungal isolate was discovered at the Regional Center for Mycology and Biotechnology (RCMB) (Leica CTR 5000, 280 DFC). Endophytic fungus was transferred to malt extract medium and cultured for 7 days at 25°C with shaking (180 rpm). Centrifugation was used to gather mycelia, and DNA was recovered. PCR amplification of purified DNA was performed using primers ITS1 and ITS4.

The sequences of fungal internal transcribed spacer ribosomal DNA (ITS-rDNA) were used to identify them. For ITS-rDNA amplification, a set of primers, ITS1 (5′-TCC GTAGGT GAA CCT GCG G-3′) and ITS4 (5′-TCC TCC GCT TGA TAT GC-3′) were employed [54], resulting in an ITS region amplicon of around 550 bp.

The BLAST software, which is accessible on the National Center for Biotechnology Information website, was used to examine sequence data in the Gene Bank database (http://www.ncbi.nlm.nih.gov). To examine DNA similarities, the unknown sequence was compared to all of the sequences in the database [55]. Bio Edit software was used to assess alignment and molecular phylogeny. The PCR results for the isolate under examination

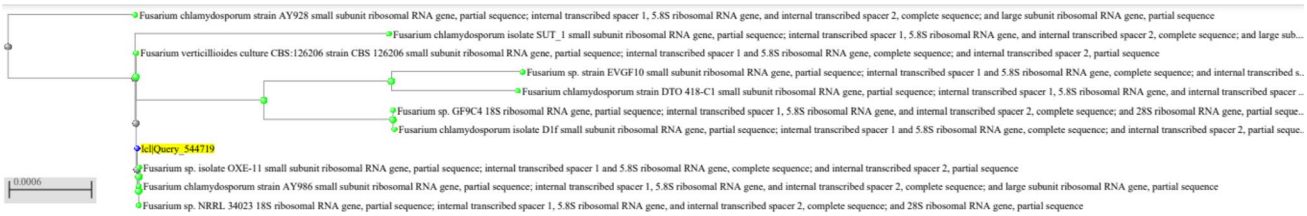


Fig. 1 *Fusarium chlamydosporum* endophytic fungus phylogenetic tree based on 18S r-RNA sequencing (yellow highlighted)

Table 1 The results of the molecular identification of *Fusarium chlamydosporum* endophytic fungus using 18S rRNA

Accession number	Identification	Accession number isolated by high similarity	Highly similarity isolates	Identity %
MW341592.1	*Fusarium chlamydosporum* isolate	MH863977.1	Fusarium verticillioides culture CBS:126206 strain CBS small subunit ribosomal RNA gene 126206, partial sequence	99.81%

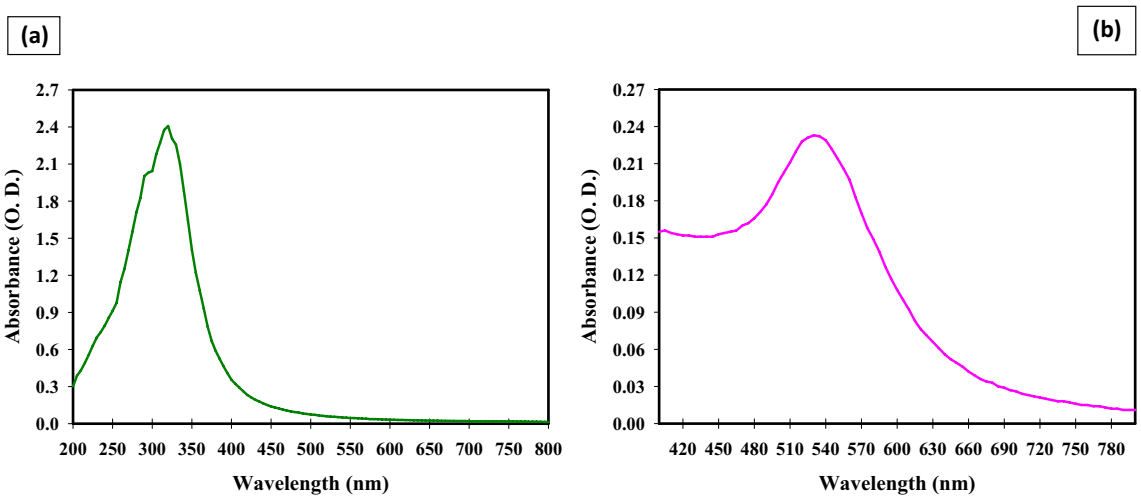


Fig. 2 UV-Vis. spectrum of **a** ZnO NPs and **b** Au NPs

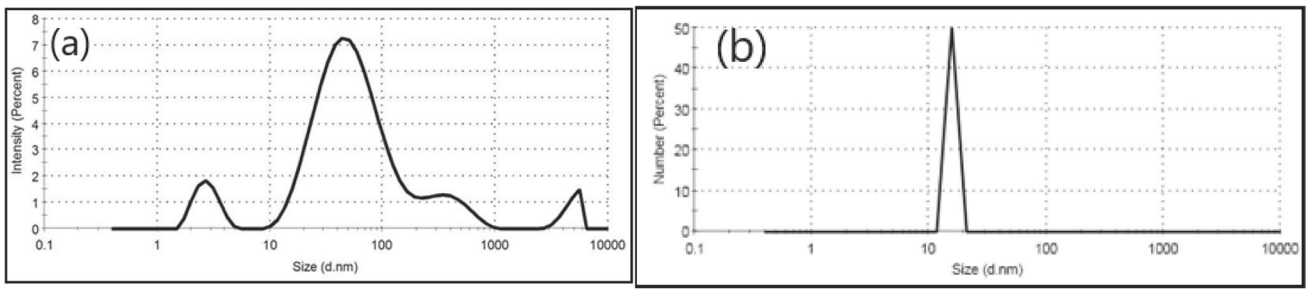


Fig. 3 Determination of particle size distribution by DLS analysis where **a** for Au NPs and **b** for ZnO NPs

were purified and sequenced at the Sigma Company of Scientific Service.

2.7 Fungal biomass preparation

On a rotary shaker (120 rpm), all fungi were cultivated for 96 h on malt extract broth at 28 °C. The biomasses were collected by filtering them using Whatman filter paper no. 1 and then washing them in distilled water to remove any medium components. The biomass (25 g wet weight) was placed in separate flasks with 100 mL of deionized water and incubated for 24 h as previously described. The biomass was filtered, and the cell filtrate was collected and used to create nanoparticles [56].

2.8 Biosynthesis of gold and zinc oxide nanoparticles

The complete synthesis of ZnO and Au NPs was performed after about 1 mL of Zn SO_4 (0.1 M), and $HAuCl_4$ (0.1 M) were separately added to 10 mL of fungal filtrate, and the solutions were agitated for 24 h in the dark at room temperature [57]. Initial characterization of produced NPs as UV-Vis spectrum of extracts depicts the green synthesis processes of ZnO NPs and Au NPs [58].

2.9 Characterization of the synthesized NPs

Ocean Optics USB2000+VIS-NIR fiber optics spectrophotometer was used to acquire absorption spectra. The color change of cell-free filtrate when combined with Zn SO_4 and $HAuCl_4$ solutions was determined at wavelengths ranging from 300 to 800 nm [59]. The fungal supernatant was used as a blank.

The transmission electron microscopy (HR-TEM) pictures were taken at the Nanotech Company for Photo-Electronic, Dreamland, Egypt, on the 6th of October city. The HRTEM is a JOEL JEM-2100 at 200 kV with a Gatan digital camera Erlangshen ES500. Sample photos were obtained in order to clearly demonstrate the particle makeup. X-ray diffraction (XRD) patterns were created using an XPERT-PRO Powder Diffractometer system, with 2 Theta (20°–80°), with minimum step size 2 Theta 0.001, and a wavelength (Ka) of 1.54614°.

The energy-dispersive X-ray (EDX) analysis is determined using an X-Max 80 detector unit equipped with a JEM-1230 transmission electron microscope for the detection of unique X-rays for elemental analysis (TEM) [60]. A Zeta-sizer (Model: Malvern Nano ZS Nano) dynamic light scattering (DLS) system equipped with a red (633 nm) laser and an Avalanche photodiode detector (APD) (quantum efficiency > 50% at 633 nm) were used to determine the hydrodynamic diameter (HD) and Zeta-potential (Malvern

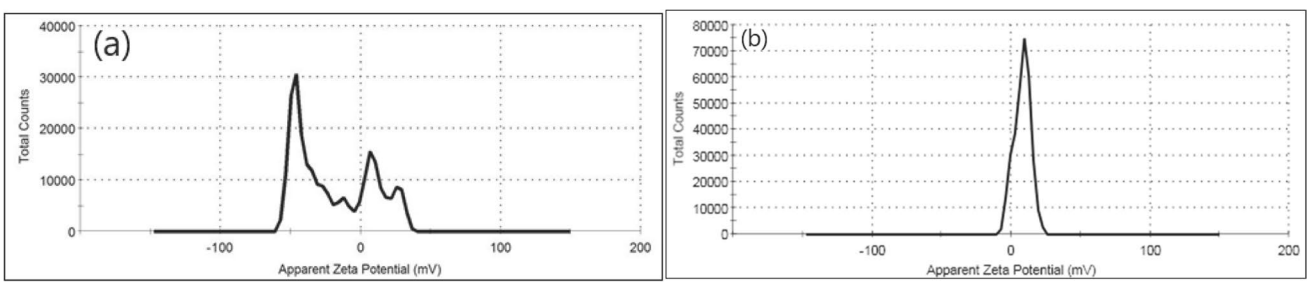


Fig. 4 Determination of surface charge and stability by ZP analysis where **a** for Au NPs and **b** for ZnO NPs

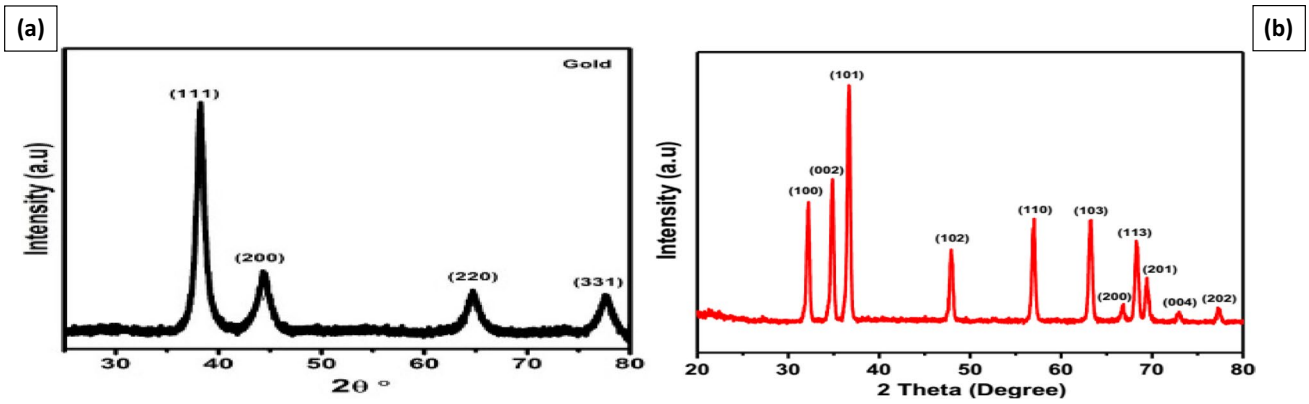


Fig. 5 XRD analysis for **a** Au NPs and **b** ZnO NPs

Instruments Ltd., England). The samples were diluted 10 times with deionized water before being measured, and 250 ml of the suspension was transferred to a disposable low volume cuvette. After equilibration to a temperature of 25°C for 2 min, five measurements were taken using 12 runs of 10 s each [61].

2.10 Antibacterial activity of the biosynthesized Au NPs and ZnO NPs

Two Gram-negative MDR bacteria, *Escherichia coli* BAA-199 and *Pseudomonas aeruginosa* BAA-2112, were tested for antibacterial activity of the biosynthesized Au NPs and ZnO NPs against harmful bacteria. The MIC is the lowest antibacterial agent concentration that can suppress bacterial growth [62]. According to Clinical and Laboratory Standards Institute (CLSI) recommendations, the MIC of biosynthesized Au NPs and ZnO NPs against bacteria was evaluated in a 96-well microtiter plate using 2,3,5-triphenyl tetrazolium chloride [63, 64], with some modifications from a previously described method by Ashengroph et al. [65].

In brief, the bacterial culture was cultivated until it reached a McFarland standard of 0.5. Following that, 10 µL of bacterial suspension was pipetted into wells containing 140 µL of nutritional broth with varying quantities of ZnO NPs and Au NPs (0.12 to 31.25 µg/mL). As a control, nutrient broth without ZnO NPs and Au NPs was provided. The microtiter plate was incubated at 37°C for 24 h [66]. After that, 10 µL of 2, 3, 5-triphenyl tetrazolium chloride solution (20 mg/mL) was added to each well and incubated for 3 h at 37 °C [67]. The MIC value was investigated in wells that did not produce a red color [68]. The measurements were taken in triplicate, and the average values SD were computed. The well-known and efficient antibiotic (AMC; amoxicillin/clavulanic acid) was used for positive control.

2.11 Cytotoxic effects of Au NPs and ZnO NPs

2.11.1 Cell line propagation

The cells were grown in Dulbecco's modified Eagle's medium (DMEM) supplemented with 10%

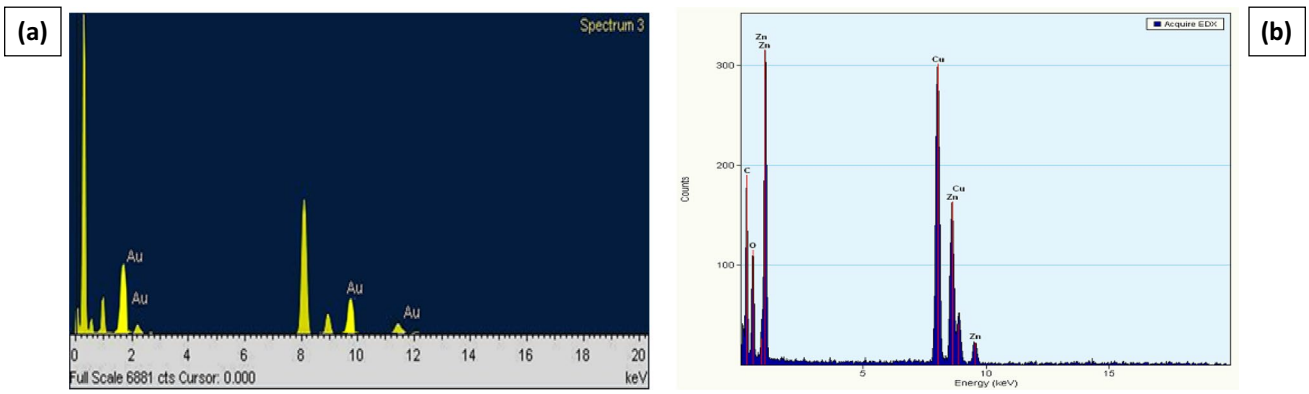


Fig. 6 EDX analysis for **a** Au NPs and **b** ZnO NPs

heat-inactivated fetal bovine serum, 1% L-glutamine, HEPES buffer, and 50 µg/ml gentamycin. All cells were grown twice a week at 37°C in a humidified atmosphere with 5% CO_2 [69].

2.11.2 Cytotoxicity evaluation using viability assay

For the cytotoxicity experiment, the cells were planted in a 96-well plate with 1×10^4 cells per well in 100 µl of growth medium. After 24 h, new medium containing varying amounts of the test sample (ZnO NPs, and Au NPs) were introduced. A multichannel pipette was used to apply repeated twofold dilutions of the tested chemical component to confluent cell monolayers in 96-well flat-bottomed microtiter plates (Falcon, NJ, USA).

The microtiter plates were incubated in a humidified incubator with 5% CO_2 for 24 h at 37°C. Three wells were used for each concentration of the test material (ZnO NPs, and Au NPs). Control cells were grown in the presence or absence of test sample and DMSO. The experiment was unaffected by the modest amount of DMSO (maximum 0.1%) included in the wells. After 24 h of incubation at 37°C, the viable cell yield was determined using a colorimetric method. The absorbance at 490 nm was measured, and the percentage of living cells was calculated using the following equation.

$$\%\text{of viability} = \frac{\text{(mean optical density of the tested sample after treatment)}}{\text{The average optical density of untreated cells.}} \times 100\cdot$$

2.12 Statistical analysis

ANOVA in one-way Duncan's multiple regions and the least significant difference (LSD) report were used to statistically analyses the choices at P 0.05 [70]. Using SPSS software (version 15), analyses and evaluations of the data and findings were conducted. All the experiments were performed in triplicate.

Table 2 MICs of different prepared NPs (ZnO, and Au NPs) against *P. aeruginosa*

Sample conc. (µg/ml)	ZnO NPs		Au NPs	
	Inhibitory percentage (%) ± SD			
	Mean of inhibitory %	SD	Mean of inhibitory %	SD
31.25	100	–	100	–
15.63	100	–	100	–
7.81	100	–	100	–
3.9	100	–	79.14	0.58
1.95	100	–	62.14	1.3
0.98	86.27	0.92	48.16	0.58
0.49	51.43	1.1	27.34	0.41
0.24	39.31	0.81	11.93	0.63
0.12	14.32	0.42	5.14	1.3
0	0	–	0	-
LSD	1.3333		0.5555	
MIC (µg/ml)	1.95		7.81	

3 Results and discussion

3.1 Endophytic fungi-assisted green synthesis of ZnO NPs and Au NPs

Our study was ongoing by isolation of fungal endophytes from leaves of *Eucalyptus sideroxylon* plant, the fungi grown out from plant tissues, were separated into pure culture on PDA. Endophytic fungi are an exceptional source of natural bioactive compounds utilized in medicine and food industry moreover; they were used in the synthesis of different nanomaterials [71].

For screening the potentiality of the isolated endophytic fungi for extracellular biosynthesis of ZnO NPs and Au NPs, aqueous solution of Zn SO_4 (0.1 M) and $HAuCl_4$ (0.1 M) were mixed with their corresponding

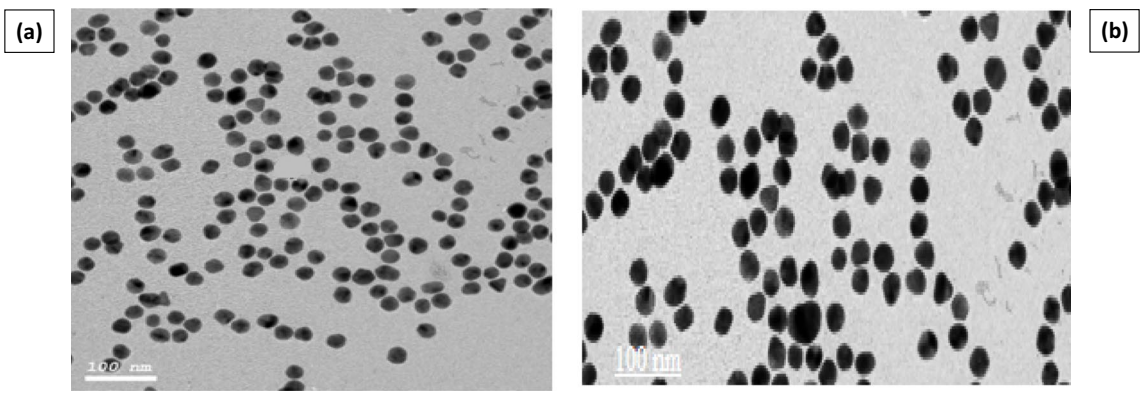


Fig. 7 Determination of shape and size by TEM imaging analysis where **a** for Au NPs and **b** for ZnO NPs

filtrates. After the complete incubation, the colors of the fungal filtrate was changed from light yellow to off-white, and purple after mixing with Zn SO_4 and $HAuCl_4$ solutions, respectively, and this observation analysis was a preliminary identification for NP formation [59].

From 13 fungal isolates (from FI-01 to FI-013), only one fungal isolate FI-03 was the most potent fungal strain for synthesis of both ZnO NPs and Au NPs, then it was identified at the Regional Center for Mycology and Biotechnology (RCMB) using image analysis system (Leica CTR 5000, 280 DFC).

The isolated fungus was recognized as *Fusarium chlamydosporum* based on macroscopic and microscopic traits, as well as molecular identification by 18S rRNA, as shown in Fig. 1. As stated in Table 1, the DNA sequencing findings were submitted to GenBank with the accession number MW341592.1.

By conducting a comparative study with Kumaravel J. [72], the fungal metabolites produced by *Metarhizium anisopliae* have a larger concentration and aid in the biological synthesis of NPs by reducing zinc and copper ions. Fungal extract's primary active metabolites participate in the biogenic synthesis of different NPs through bio-reduction of their corresponding ions [73].

Based on Šebesta and Vojtková [74], the fungal filtrate contains enzymes with the capacity to convert metal ions to elemental metal (M°). Biomolecules can interact with metal ions to create intricate electron transport pathways during the production of metals, in which NADPH/NADH transform into $NADP^+$/NAD^+ [75, 76]. Fungal synthesis of NPs is a simple and straightforward method due to the simplicity of subsequent processing and biomass procedures, as well as better productivity than bacteria [66, 77].

Table 3 MICs of different prepared NPs (ZnO, and Au NPs) against *E. coli*

Sample conc. (µg/ml)	ZnO NPs		Au NPs	
	Inhibitory percentage (%) ± SD			
	Mean of inhibitory %	SD	Mean of inhibitory %	SD
31.25	100	–	100	–
15.63	100	–	100	–
7.81	100	–	100	–
3.9	100	–	100	–
1.95	100	–	71.32	0.96
0.98	100	–	49.82	1.3
0.49	100	–	31.91	0.58
0.24	79.35	1.3	17.34	1.3
0.12	51.63	0.58	5.62	0.47
0	0	–	0	–
LSD	1.3333		0.6000	
MIC (µg/ml)	0.98		3.9	

3.2 Characterization of biogenic ZnO NPs, and Au NPs

3.2.1 UV-Vis. absorption spectra

The excitonic absorption peaks were between 300 and 400 nm, which are typical for ZnO NP peak and hence establish their existence. The maximum absorption peak of the synthesized ZnO NPs was 320 nm, demonstrating the synthesis of ZnO in the nano-form (Fig. 2a); this finding is in good agreement with the previously reported values [78], and consistent with recent findings showing ZnO NPs have a maximum absorbance wavelength in the region of 300–400 nm [79, 80].

Additionally, Au NPs have a maximum absorbance peak at 530 nm. A single, prominent absorption peak in the spectra confirms the existence of metallic Au NPs (Fig. 2b). This finding agrees with the references [81, 82]. A convincing spectroscopic signal of their manifestation was supplied by the produced light's off-white and pink colors, which were attributed to the activation of the surface plasmon resonance of biogenic ZnO NPs and Au NPs, respectively [83].

The off-white and purple colors' intensity matched the produced fungal filtrate's capacity to biosynthesize ZnO NPs and Au NPs, respectively [84, 85]. Surface plasmon resonance (SPR) is often influenced by the intensity, size, morphology of the present surfaces, arrangement, and dielectric characteristics of any produced NPs [86, 87].

3.2.2 Dynamic light scattering analysis

A common approach for assessing particle size in colloidal solution is dynamic light scattering. It is used to calculate the thickness of the shell of a capping or stabilizing chemical encapsulating the metallic NPs as well as the actual particle size distribution of the metallic core [88].

According to DLS results, the hydrodynamic diameter (HD) of Au NPs and ZnO NPs is approximately 34.88 nm (Fig. 3a) and 15.77 nm (Fig. 3b), respectively, and their corresponding polydispersity index (PDI) was approximately 0.77, and 0.952, which attributed to the highest tendency to be aggregated based on their hydrophilicity nature (Fig. 3a, b).

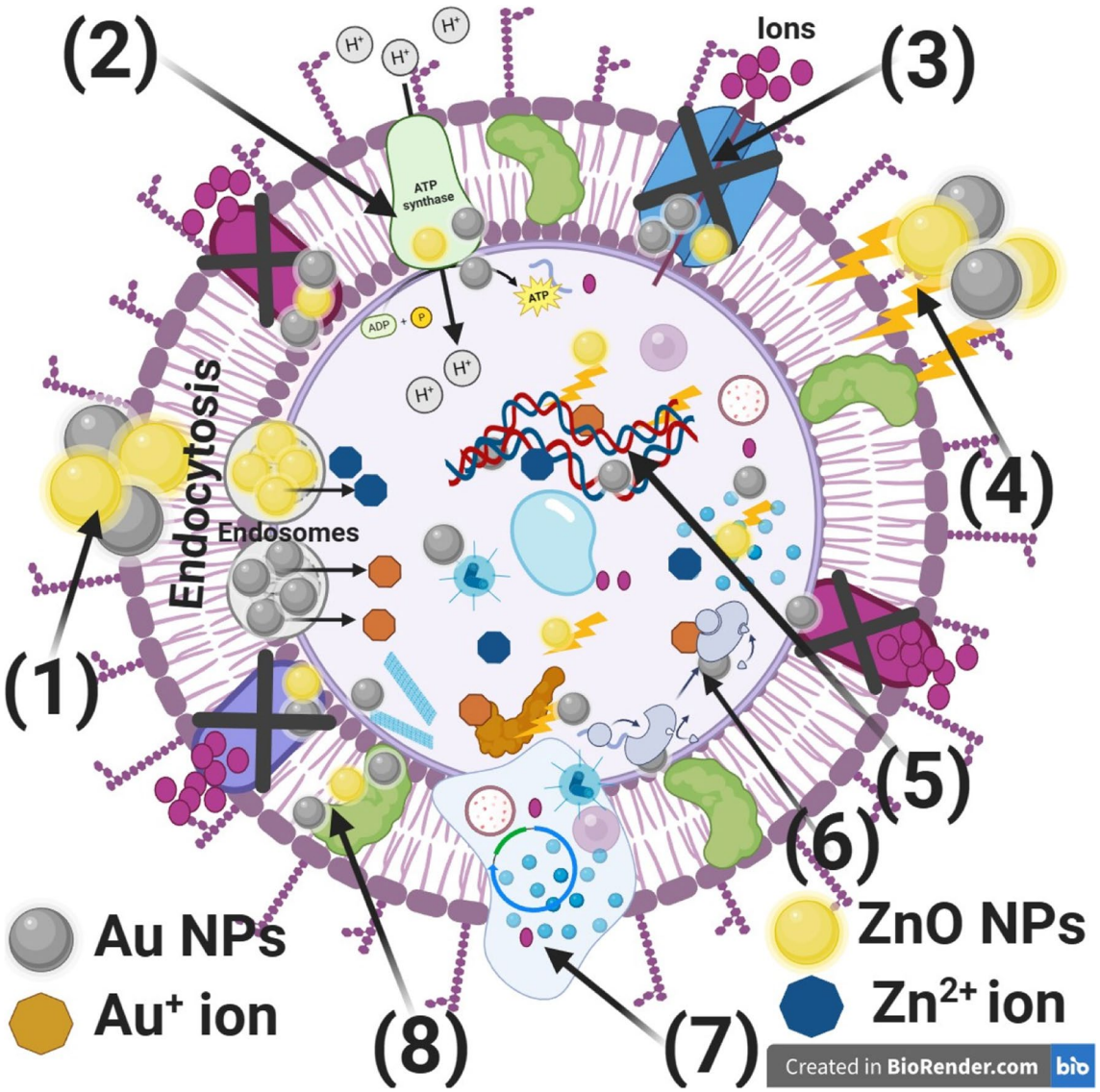


Fig. 8 Illustrates the expected reaction mechanisms of the biogenically synthesized ZnO NPs, and Au NPs against bacterial cell, where (1) ZnO NPs and Au NPs adhere to the bacterial cell surface and result in membrane breakdown, endocytosis, the creation of endosomes, and altered transport potential; (2) ZnO NPs and Au NPs damage the electron transport chain; (3) ZnO NPs and Au NPs prevent ions from entering and leaving the bacterial cell; (4) ZnO NPs and Au NPs produce and increase ROS, which suggests that the bacterial cell wall is weakening; (5) ZnO NPs and Au NPs enter bacterial cells and interact with cellular organelles (such as DNA), affecting the function of the corresponding cellular components and triggering cell lysis; (6) ZnO NPs and Au NPs interact with enzymes and metabolism; (7) ZnO NPs and Au NPs disrupt the cell membrane and resulting in the leakage of the internal organelles; and (8) ZnO NPs and Au NPs inhibit the membrane protein. Additionally, ZnO NPs and Au NPs could act as a transporter to effectively release Zn^{2+} and Au^{+} ions into the cytoplasm and layer, where the presence of proton motive force would cause the pH to drop below 3.0 and encourage the release of Zn^{2+} and Au^{+} ions. The figure created by BioRender.com

The particle size stabilized NPs were determined using DLS analysis of the produced NPs, and the NPs produced had an average diameter of 40 to 45 nm which matched with the results of Clarance et al. [89].

The NPs that were produced in our study were greatly dispersed in a narrow and uniform size as a result of the scientific validity of DLS, which successfully improved their characteristics and applications [90].

3.2.3 Zeta potential analysis

The synthesized NPs' surface charge and stability were assessed using zeta potential (ZP) analysis.

The magnitude of ZP reflects a colloid's potential stability, with an average ZP value of 37.6 for Au NPs (Fig. 4a), and 8.01 for ZnO NPs as shown in Fig. 4b.

Table 4 Cytotoxicity evaluation of different NPs against colon cancer (HCT-116) cell line

Conc. of NPs (µg/ml)	Viability % in presence of Au NPs	Viability % in presence of ZnO NPs
0	100 ± 5.0	100 ± 8.1
0.05	100 ± 9.0	100 ± 8.3
0.1	100 ± 8.0	100 ± 6.8
0.2	100 ± 7.1	100 ± 4.6
0.39	100 ± 6.8	100 ± 6.2
0.78	97.49 ± 5.8	98.42 ± 6.0
1.56	89.13 ± 2.3	85.16 ± 5.7
3.125	70.68 ± 3.1	63.74 ± 3.7
6.25	47.52 ± 4.1	41.55 ± 5.5
12.5	31.89 ± 3.1	28.94 ± 2.8
25	17.93 ± 2.2	16.43 ± 1.8
50	7.48 ± 1.8	7.59 ± 1.4
100	3.62 ± 1.3	4.61 ± 1.2
IC_{50}	5.92	5.06

If particles have small zeta potential values, they resist each other and there is no aggregation; however, if particles have high negative or positive zeta potential values, there is no force to prevent particle coming together and aggregation.

In Tripathi et al.'s [91] study, Au NPs having a zeta potential of 35.9 mV may be stored for up to 2 months without losing quality or stability. The ideal value of ZnO zeta potential, according to Almukainzi et al. [92], ranges from +40 to −40 mV to ensure adequate dispersibility with no risk of aggregation or flocculation [92].

Table 5 Cytotoxicity evaluation of different NPs against intestinal cancer (CACO2) cell line

Conc. of NPs (µg/ml)	Viability % in presence of Au NPs	Viability % in presence of ZnO NPs
0	100 ± 5.1	100 ± 5.4
0.05	86.41 ± 8.4	100 ± 7.7
0.1	81.73 ± 7.8	100 ± 6.9
0.2	71.39 ± 6.9	100 ± 5.4
0.39	62.50 ± 5.8	96.03 ± 4.9
0.78	54.89 ± 6.6	87.24 ± 5.6
1.56	43.12 ± 3.3	70.81 ± 4.6
3.125	36.08 ± 2.8	54.12 ± 4.3
6.25	28.65 ± 3.7	32.39 ± 2.9
12.5	20.97 ± 3.7	21.47 ± 3.3
25	11.46 ± 2.4	10.81 ± 4.3
50	5.19 ± 2.5	6.53 ± 2.9
100	2.34 ± 2.5	2.74 ± 3.5
IC_{50}	1.1	6.07

3.2.4 XRD analysis

According to the XRD pattern of as-prepared Au NPs, the face-centered cubic (fcc) structure of gold is the prevalent crystallographic structure (Joint Committee on Powder Diffraction Standards-JCPDS No. 04-0784). The diffraction peaks found at 2 θ = 38.31° (111), 43.46° (200), 64.67° (220), and 77.45° (311) are the same as those reported for standard gold metal (Au°). As shown in Fig. 5a, the XRD pattern indicates that the Au NPs were largely crystalline, as confirmed by Soni and Prakash [93].

The hexagonal shape is the most predominate crystallographic structure in the as-prepared ZnO NPs, as seen by the XRD pattern (JCPDS No. 79-0205). The hexagonal structure was verified by the diffraction peaks with 2 θ =31.76° (100), 34.58° (002), 36.67° (101), 47.89° (102), 57.01° (110), 63.29° (103), 66.67° (200), 68.25° (112), 69.35° (201), 73.27° (004), and 77.26° (202). In this case, no other impurity peaks are observed in the XRD patterns, suggesting that all products are relatively pure NPs, as shown in Fig. 5b, which is consistent with earlier results of Faisal et al. [94], and Koutu et al. [95].

The generated NPs were highly crystalline and conjugated with amorphous fungal filtrate, which increased their dispersion in the solution for improved biomedical application, according to the XRD data analysis [96].

3.2.5 EDX analysis

The EDX method is frequently used to get quantitative elemental information. The investigation of Au NPs with energy-dispersive X-rays revealed an optical absorption band peak at roughly 2.2 keV (Fig. 6a), which is typical of metallic gold nanocrystallites' absorption [97].

As demonstrated in Fig. 6b, the element mappings demonstrate that Zn and O are blended uniformly in the spheres. The spectrum displays peaks for Zn at 1.5, 8.5, and 9.6 MeV, as well as an O peak from 0.9 to 1.1 MeV, indicating that the NPs have a ZnO structure.

Figure 6b displays the composition line profiles, and the EDX spectra revealed that the required phase of Zn and O was present in the samples, indicating the great purity of the generated ZnO NPs. In principle, the expected stoichiometric mass percent of Zn and O are 64.61 and 35.39%, respectively.

The EDX analyses in our work show identical results for both generated NPs, whereas the preceding study stated the elemental composition of zinc and oxygen as 76.9% and 23.1%, respectively [98].

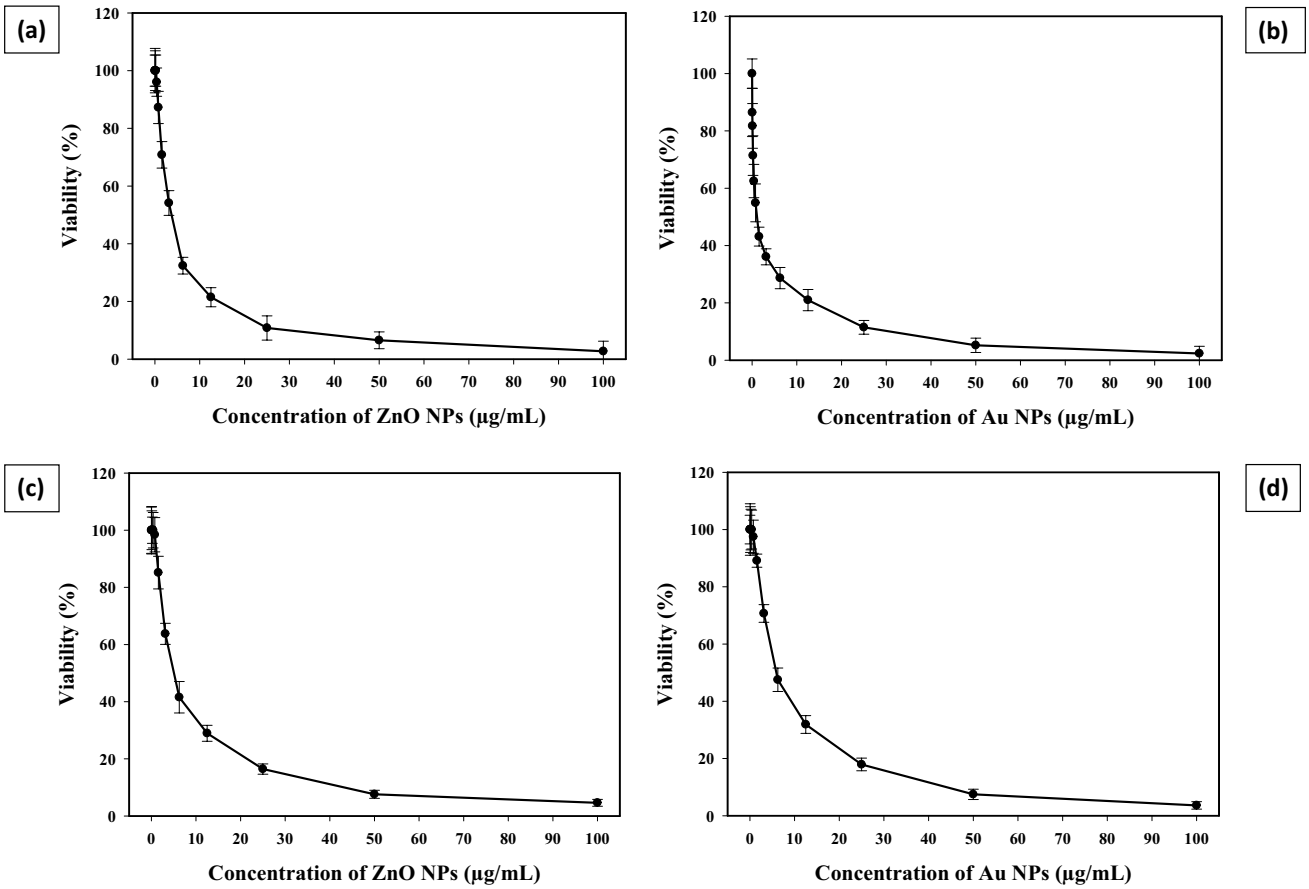


Fig. 9 Cytotoxicity evaluation of the biosynthesized ZnO NPs against CACO2 cell lines (**a**), Au NPs against CACO2 cell lines (**b**), ZnO NPs against HCT-116 cell lines (**c**), and Au NPs against HCT-116 cell lines (**d**)

3.2.6 HRTEM imaging

TEM was used to examine the size and exact shape of the synthesized NPs. The particle size of the biosynthesized Au NPs ranged between 15 and 28 nm, with an average size of 22.1 nm indicating approximately spherical and separated particles as shown in Fig. 7a and matching with Mishra et al. [99].

On the other hand, the TEM image indicated that the biosynthesized ZnO NPs were spherical and hexagonal in form, with diameters ranging from 14 to 28 nm with a mean size of 19.3 nm as shown in Fig. 7b and matching with the earlier studies [100–102].

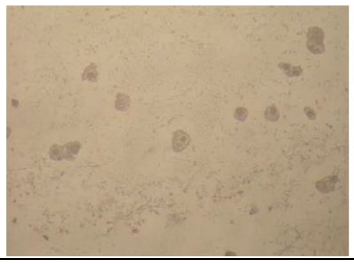
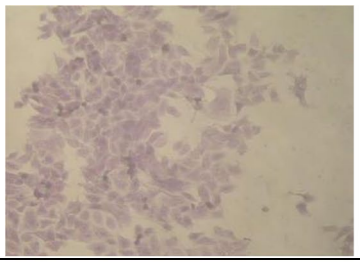
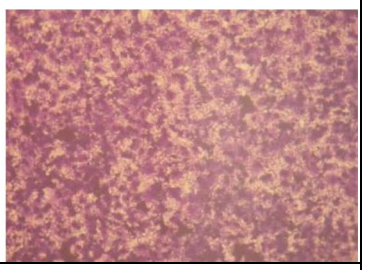
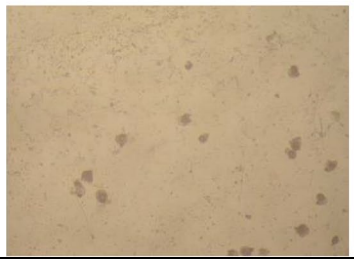
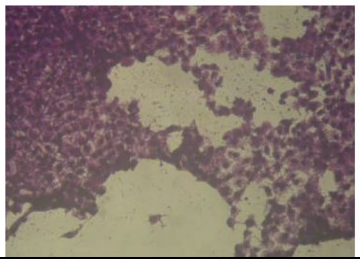
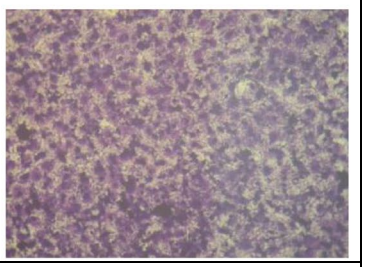
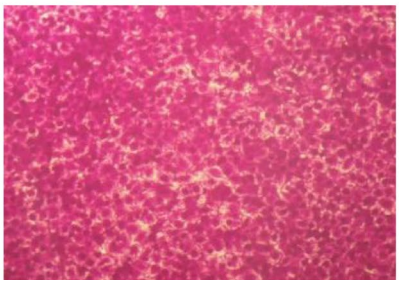
It was discovered that our synthesized NPs were polydispersed, varied in size, and mostly had spheroidal particles as their dominating shape after compared to articles in the field on intermediate particle size and form. That effort indicated in the following study [103] may have produced a variety of forms.

Although all of the newly produced NPs were sphere- or orbicular-shaped, different morphologies may have been seen as a result of the extraction-based synthetic process, which is why the anisotropic form was detected. Only the most practical reducing and capping agents (fungal filtrate) were utilized in our research; thus, a stable form is exhibited in several ways.

The findings showed that the estimated sizes of the particles identified by HRTEM imaging were smaller than the mean and prevalent sizes indicated by DLS analysis. The hydrodynamic radius of the biosynthesized ZnO NPs and Au NPs and the surrounding water layers, as well as the considerable sizes of the biosynthesized NPs, are the causes, based on the given reference [104].

By using the extract of a filamentous fungus, Castro-Longoria et al. [103] synthesized silver, gold, and silver-gold bimetallic. After the fungus was subjected to the aqueous solutions of 10^{-3} M of $AgNO_3$ and $HAuCl_4$, respectively, the shape of the NPs was found to be primarily spherical with an average diameter of 11.0 nm for silver and 32.0 nm for gold.

Table 6 Photos showed the effect of different types of biosynthetic NPs (Au NPs, and ZnO NPs; at different concentrations) against colon cancer (HCT-116) cell line

Treated biosynthesized nanoparticles	100 µg/mL	10 µg/mL	1 µg/mL
Au NPs			
ZnO NPs			
Control			

3.3 Antibacterial activity of biosynthesized Au NPs and ZnO NPs

The rise and fast spread of antibiotic-resistant bacteria pose a severe worldwide danger to human health. It is obvious that the time and principal necessary for generating new medicines is lengthy [105, 106].

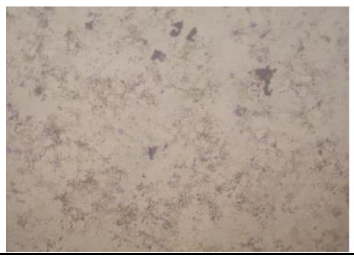
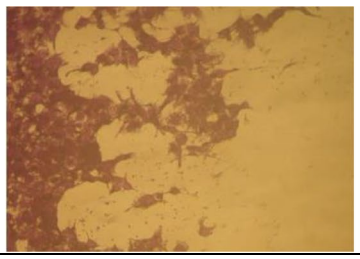
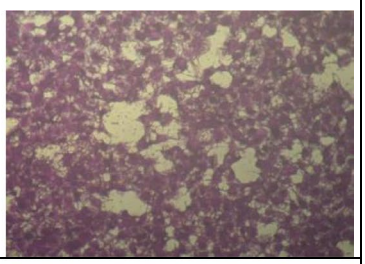
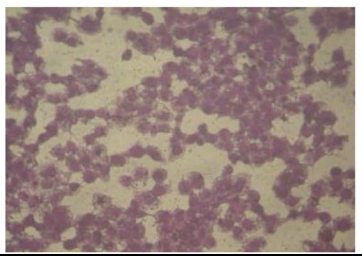
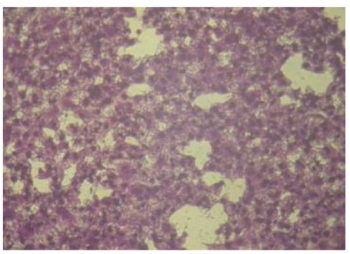
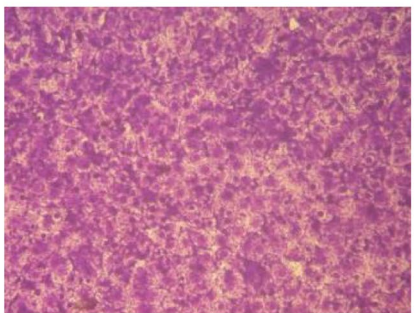
In MHB media, NPs and pathogenic *E. coli* BAA-199 and *P. aeruginosa* BAA-2112 are incubated. The inoculum bacterium concentration is roughly 1×10^5 CFU/mL. Two-fold dilutions yielded NP concentrations ranging from 0.49 to 125 µg/mL. After 24 h of incubation at 37°C, the absorbance at 540 nm, which relies on the bacterium concentration, provides evaluation of the bacteria development.

Table 2 indicates the minimum inhibitory concentration (MIC), where MICs of Au NPs and ZnO NPs against *P. aeruginosa* were 7.81 and 1.95 µg mL^{-1}, respectively, whereas Table 3 shows that the MIC of Au NPs and ZnO NPs against *E. coli* and were calculated as 3.9 and 0.98 µg mL^{-1}, respectively. It must be noted that the MICs of the positive control (AMC; standard antibacterial agent) were 15.0 µg mL^{-1} against *E. coli* and *P. aeruginosa.*

Studies show that the MIC of ZnO NPs is lower than that of Au NPs against these pathogens such as *E. coli* and *P. aeruginosa*. It was discovered that increasing ZnO NP concentration leads in a reduction in microbial cell proliferation. ZnO NP inhibitory effectiveness is affected by NP concentrations, sizes, and forms [39, 107].

P. aeruginosa and *E. coli* were both shown to be Gram-negative bacteria, and our results indicate the antibacterial activities of ZnO NPs and Au NPs at lower concentrations. Previous studies have shown excellent antibacterial activity, which is consistent with our findings [108, 109]. According to the literature review, ZnO NPs can inhibit bacterial development by disrupting the bacterial cell membrane and allowing cytoplasmic contents to leak out, ultimately leading to the bacterium's death [110].

Table 7 Photos showed the effect of different types of biosynthetic NPs (Au NPs, and ZnO NPs; at different concentrations) against intestinal cancer (CACO2) cell line

Treated biosynthesized nanoparticles	100 µg/mL	10 µg/mL	1 µg/mL
Au NPs			
ZnO NPs			
Control			

Some zinc-based nanocomposites were prepared by Al-Dhabaan et al. [111], which exhibits better antibacterial and antifungal activities. The electrostatic interaction that damages cell membranes, disrupts proteins and enzymes, produces ROS and oxidative stress, binds to proteins and disturbs homeostasis (disrupting the electron transport chain), inhibits signal transduction, and is genotoxic may be the mechanism of action of the produced NPs [16, 112]. Additionally, the effectiveness may be linked to the NPs' exterior surface's roughness, which damages cell walls and allows NPs to infiltrate plasma membranes [39].

Ibănescu [113] reported that Ag NPs and ZnO NPs had antibacterial action toward *E. coli* and *Micrococcus luteus*. Also, in other studies, Ag NPs and ZnO NPs exhibited antibacterial activity against *P. aeruginosa* and *S. aureus* [114–116].

Based on the obtained antibacterial activity results of ZnO NPs, and Au NPs, we continued to investigate the mechanism of action of ZnO NPs, and Au NPs on tested bacteria. Uncertain is the precise mechanism by which ZnO NPs and Au NPs affect cells. Figure 8 illustrates the different modes of action of ZnO NPs, and Au NPs, which include an attachment to the surface of the bacterial cell wall and membrane, penetration into the cell and disruption of intracellular organelles and biomolecules, development of oxidative stress, and modification of signal transduction pathways [88, 117, 118]. Figure 8 shows the different modes of actions of ZnO NPs and Au NPs.

3.4 Anticancer effects of biosynthesized Au NPs and ZnO NPs

The biosynthesized Au NPs and ZnO NPs' medicinal importance is particularly promising in the realm of anticancer therapy. The 50% inhibitory concentration (IC_{50}) is the concentration required to cause toxicity in 50% of unaffected cells.

Tables 4 and 5 show the least inhibitory concentrations of ZnO NPs (5.06 µg/mL and 6.07 µg/mL) and Au NPs (5.9 µg/mL and 1.1 µg/ml) against HCT-116 and CACO2 cell lines, respectively.

Toxicity of biosynthesized ZnO NPs on CACO2 cells increases as dose-dependently like 0.0, 0.05, 0.1, 0.2, 0.39, 0.78, 1.56, 3.125, 6.25, 12.5, 25, 50, and 100% µg/mL of ZnO NPs where the percentage of cell viability is reduced by 100, 100, 100, 100, 96.03, 87.24, 70.81, 54.12, 32.39, 21.4, 10.81, 6.53, and 2.74%, respectively, as shown in Fig. 9a.

Additionally, the percentage of cell viability is reduced by 100, 86.41, 81.73, 71.39, 62.5, 54.89, 43.12, 36.08, 28.65, 20.97, 11.46, 5.19, and 2.34%, respectively, when treated with the biosynthesized Au NPs as illustrated in Fig. 9b.

The same situation was observed in the toxicity of biosynthesized ZnO NPs on HCT-116 cell line where the percentage of cell viability is reduced to be finally 3.62, and 4.61% after the treatment with 100% Au NPs and ZnO NPs, respectively (see Fig. 9c, d).

Although this significant decrease in cell viability was expected at first look that make ZnO NPs is more effective against colon cancer HCT-116 than Au NPs because ZnO NPs have IC_{50} Lower than Au NPs. has also been reported in previous studies [119].

Data analysis indicated that the vitality of treated cell lines was dose dependent; as the concentration of ZnO NPs raised, the viability dropped [120]. Another study found that biogenic ZnO NPs showed cytotoxic activity against colorectal cancer cell lines (HCT-116 and CACO-2) but not against the control cell line (HEK-293) [121]. Table 6 shows some photos of the treated colon cancer (HCT-116) cell line by different biosynthesized Au NP and ZnO NP concentrations with respect to the control non-treated cells. Additionally, Table 7 shows some photos of the treated intestinal cancer (CACO2) cell line by different biosynthesized Au NPs and ZnO NPs concentrations with respect to the control non-treated cells.

The increased anticancer action of ZnO NPs and Au NPs is owing to the release of Au^{+} and Zn^{2+} ions, which resulted in ROS penetrating the cancer cell membrane and causing cell death. The generation of ROS is a key mechanism behind NPs anticancer activity [122, 123]. By using a methyl thiazolyl tetrazolium assay, Low et al. [119] demonstrated that the synthesized ZnO NPs have anticancer properties when tested against the HCT-116 human colon cancer cell lines. Higher potency ZnO NPs than those made chemically showed substantial anticancer effect against colon cancer cells [119].

According to Abolghasem et al. [124], cervical (HeLa), ovarian (Caov-4), and breast (MCF-7) cancer cell lines all exhibited anticancer activity when exposed to biologically produced Au NPs at various concentrations [124]. Au NPs are currently becoming more well known for their application in the detection and treatment of cancer.

On cancer cells, Au NP conjugations with adamantane and cyclodextrins appear to have photothermal effects [125]. According to a research by Hamed et al. [126], biosynthesized Au NPs used in the study demonstrated successful antibacterial and anticancer properties [126].

Similar investigations demonstrated that equivalent IC_{50} values of 2.7 µg/mL were achieved. Over the normal cell lines, the particles, however, were shown to be innocuous [127]. The control cells, however, had typical intact cell morphology.

Other investigations also noted substantial modifications in cancer cell shape following treatment with ZnO NPs [120]. Because of their lower IC_{50} values, green ZnO NPs have a higher anticancer potential, according to our data.

Ambujakshi and Raveesha [128] reported biosynthesized Ag and ZnO NPs using *Chonemorpha grandiflora* leaf extract MCF 7, HCT 116, and A 549 cell lines. Additionally, Elsayed and Alomari [129] fabricated ZnO and Ag NPs using laser ablation and found these particles have anticancer activity against HCT-116 and HELA cancerous cell lines.

Finally, Pandiyan and Murugesan [130] reported that the nanocomposite (Ag-Au/ZnO) has potential anticancer activity toward human cervical cancerous cells (HeLa).

4 Conclusion

Fusarium chlamydosporum MW341592 can be used to biosynthesis ZnO NPs and Au NPs without the use of hazardous chemical reagents by a cost-effective, non-toxic, and ecofriendly method. The biosynthesized ZnO NPs and Au NPs were pure, mostly spherical, and averaged 19.3 nm and 22.1 nm in size, respectively. The magnitude of ZP reflects a colloid's potential stability, with an average ZP value of 37.6 for Au NPs and 8.01 for ZnO NPs. The biosynthesized ZnO NPs efficiently suppressed the growth of Gram-negative bacteria *E. coli* at MIC = 0.98 µg/mL and *P. aeruginosa* at MIC = 1.95 µg/mL, more than the biosynthesized Au NPs making ZnO NPs a promising antibacterial agent. It was founded that increasing ZnO NP concentration leads in a reduction in microbial cell proliferation, and the inhibitory potential is affected by their concentrations, sizes, and shape. The anticancer results indicate that the least inhibitory concentrations for ZnO NPs were 5.06 µg/mL and 6.07 µg/mL and for Au NPs were 5.92 µg/mL and 1.1 µg/ml against

HCT-116 and CACO2 cell lines, respectively. Toxicity of biosynthesized ZnO NPs on CACO2 cells increases as dose-dependently like 0.0, 0.05, 0.1, 0.2, 0.39, 0.78, 1.56, 3.125, 6.25, 12.5, 25, 50, and 100% µg/mL of ZnO NPs where the percentage of cell viability is reduced by 100, 100, 100, 100, 96.03, 87.24, 70.81, 54.12, 32.39, 21.4, 10.81, 6.53, and 2.74%, respectively. The biosynthesized ZnO NPs and Au NPs like almost active polymeric materials will be the key to overcoming the limitations of other bactericidal substances such as some resistant substances and drugs. Antimicrobial and anticancer biomaterials, their unique combinations, and the methodologies now under development will pave the way for a bright future in infection and cancer therapies. Therefore, the activities of the biosynthesized ZnO NPs and Au NPs against the virulence factors of some pathogenic bacteria make treatment options much easier compared to the challenge represented by the exceptional ability of pathogenic bacteria to acquire resistance. To fully comprehend the mechanism underlying biosynthesized ZnO NPs and Au NPs and antibacterial and anti-cancerous effects, as well as their potential genotoxicity, more research is necessary.

Author contribution SEH suggested the research topic, investigated the article, planned the research methodology, wrote the original draft, and participated in data representation and article revising and editing. MNE suggested the research topic, investigated the article, planned the research methodology, wrote the original draft, and participated in data representation and article revising and editing. MMA suggested the research topic, investigated the article, planned the research methodology, wrote the original draft, and participated in data representation and article revising and editing. GSE suggested the research topic, investigated the article, planned the research methodology, wrote the original draft, and participated in data representation and article revising and editing. HHE suggested the research topic, investigated the article, planned the research methodology, wrote the original draft, and participated in data representation and article revising and editing.

Funding Open access funding provided by The Science, Technology & Innovation Funding Authority (STDF) in cooperation with The Egyptian Knowledge Bank (EKB).

Data availability The datasets used and analyzed during the current study are available from the corresponding author on reasonable request.

Declarations

Research involving human participation and/or animals Not applicable.

Ethical approval Not applicable.

Informed consent Not applicable.

Conflict of interest The authors declare no competing interests.

Open Access This article is licensed under a Creative Commons Attribution 4.0 International License, which permits use, sharing, adaptation, distribution and reproduction in any medium or format, as long as you give appropriate credit to the original author(s) and the source, provide a link to the Creative Commons licence, and indicate if changes were made. The images or other third party material in this article are included in the article's Creative Commons licence, unless indicated otherwise in a credit line to the material. If material is not included in the article's Creative Commons licence and your intended use is not permitted by statutory regulation or exceeds the permitted use, you will need to obtain permission directly from the copyright holder. To view a copy of this licence, visit http://creativecommons.org/licenses/by/4.0/.

References

1. Bray F et al (2021) The ever-increasing importance of cancer as a leading cause of premature death worldwide. Cancer 127(16):3029–3030
2. Ferlay J et al (2018) Global cancer observatory: cancer today. Lyon, France: International Agency for Research on Cancer 3(20), https://gco.iarc.fr/today/home
3. Chidambaram M, Manavalan R, Kathiresan K (2011) Nanotherapeutics to overcome conventional cancer chemotherapy limitations. J Pharm Pharm Sci 14(1):67–77
4. Nabil A et al (2020) Zinc oxide nanoparticle synergizes sorafenib anticancer efficacy with minimizing its cytotoxicity. Oxidative Med Cell Longev. https://doi.org/10.1155/2020/1362104
5. Islam F et al (2022) Exploring the journey of zinc oxide nanoparticles (ZnO-NPs) toward biomedical applications. Materials 15(6):2160
6. Herszenyi L, Tulassay Z (2010) Epidemiology of gastrointestinal and liver tumors. Eur Rev Med Pharmacol Sci 14(4):249–258
7. Society AC (2014) Cancer facts & figures. Am Cancer Soc 2014. https://www.cancer.org/research/cancer-facts-statistics/all-cancer-facts-figures/cancer-facts-figures-2014.html
8. De Flora S, La Maestra S (2015) Epidemiology of cancers of infectious origin and prevention strategies. J Prev Med Hyg 56(1):E15
9. Safdar A, Armstrong D (2001) Infectious morbidity in critically ill patients with cancer. Crit Care Clin 17(3):531–570
10. Oliveira A et al (2007) Epidemiology of bacteremia and factors associated with multi-drug-resistant gram-negative bacteremia in hematopoietic stem cell transplant recipients. Bone Marrow Transplant 39(12):775–781
11. Markou P, Apidianakis Y (2014) Pathogenesis of intestinal Pseudomonas aeruginosa infection in patients with cancer. Front Cell Infect Microbiol 3:115
12. Viscoli C, Varnier O, Machetti M (2005) Infections in patients with febrile neutropenia: epidemiology, microbiology, and risk stratification. Clin Infect Dis 40(Supplement_4):S240–S245
13. Patel HG, Tabassum S, Shaikh S (2017) E. coli sepsis: red flag for colon carcinoma—a case report and review of the literature. Case Rep Gastroentero Med. https://doi.org/10.1155/2017/2570524
14. Hernández-Luna MA, Lagunes-Servin HE, Lopez-Briones S (2016) The role of Escherichia coli in the development and progression of cancer. ARC J Cancer Sci 3(1):1–11
15. Buc E et al (2013) High prevalence of mucosa-associated E. coli producing cyclomodulin and genotoxin in colon cancer. PloS One 8(2):e56964
16. Baptista PV et al (2018) Nano-strategies to fight multidrug resistant bacteria—"A Battle of the Titans". Front Microbiol 9:1441
17. Abdelfattah NA et al (2023) Influence of biosynthesized magnesium oxide nanoparticles on growth and physiological aspects for cowpea (Vigna unguiculata L.) plant, cowpea beetle, and cytotoxicity. Biotechnol J. https://doi.org/10.1002/biot.202300301

18. Mohd Yusof H et al (2019) Microbial synthesis of zinc oxide nanoparticles and their potential application as an antimicrobial agent and a feed supplement in animal industry: a review. J Anim Sci Biotechnol 10:1–22
19. Zak AK et al (2011) Synthesis and characterization of a narrow size distribution of zinc oxide nanoparticles. Int J Nanomedicine 6:1399–1403. https://doi.org/10.2147/IJN.S19693
20. Hashem AH et al (2022) Synthesis of chitosan-based gold nanoparticles: antimicrobial and wound-healing activities. Polymers 14(11):2293
21. Moyer E, Hardon A (2014) A disease unlike any other? Why HIV remains exceptional in the age of treatment. Med Anthropol 33(4):263–269
22. Mozaffari H et al (2016) Prevalence of oral and pharyngeal cancers in Kermanshah province, Iran: a ten-year period. Int J Cancer Res 12(3-4):169–175
23. Imani MM, Safaei M (2019) Optimized synthesis of magnesium oxide nanoparticles as bactericidal agents. J Nanotechnol. https://doi.org/10.1155/2019/6063832
24. Wong CY, Al-Salami H, Dass CR (2017) Potential of insulin nanoparticle formulations for oral delivery and diabetes treatment. J Control Release 264:247–275
25. Sharifi R et al (2017) Effect of massage on the success of anesthesia and infiltration injection pain in maxillary central incisors: double-blind, crossover trial. Dent Hypotheses 8(3):61
26. Mozaffari HR et al (2019) Serum and salivary interleukin-4 levels in patients with oral lichen planus: a systematic review and meta-analysis. Oral Surg Oral Med Oral Pathol Oral Radiol 128(2):123–131
27. Chen W-Y et al (2010) Functional gold nanoclusters as antimicrobial agents for antibiotic-resistant bacteria. Nanomedicine 5(5):755–764
28. Albanese A, Tang PS, Chan WC (2012) The effect of nanoparticle size, shape, and surface chemistry on biological systems. Annu Rev Biomed Eng 14:1–16
29. Arshad A et al (2017) Graphene/SiO2 nanocomposites: the enhancement of photocatalytic and biomedical activity of SiO2 nanoparticles by graphene. J Appl Phys 121:24
30. Shah M et al (2015) Green synthesis of metallic nanoparticles via biological entities. Materials 8(11):7278–7308
31. Ijaz F et al (2017) Green synthesis of copper oxide nanoparticles using Abutilon indicum leaf extract: antimicrobial, antioxidant and photocatalytic dye degradation activitie. Trop J Pharm Res 16(4):743–753
32. Mukherjee P et al (2008) Green synthesis of highly stabilized nanocrystalline silver particles by a non-pathogenic and agriculturally important fungus T. asperellum. Nanotechnology 19(7):075103
33. Chopra H et al (2022) Green metallic nanoparticles: biosynthesis to applications. Front Bioeng Biotechnol 10:548
34. Baker S, Satish S (2015) Biosynthesis of gold nanoparticles by Pseudomonas veronii AS41G inhabiting Annona squamosa L. Spectrochim Acta A Mol Biomol Spectrosc 150:691–695
35. Rana KL et al (2020) Endophytic microbes in nanotechnology: current development, and potential biotechnology applications, in Microbial endophytes. Elsevier, pp 231–262
36. Vuong QV et al (2015) Physicochemical, antioxidant and anticancer activity of a Eucalyptus robusta (Sm.) leaf aqueous extract. Ind Crop Prod 64:167–174
37. Hashem AH et al (2023) Unveiling anticancer, antimicrobial, and antioxidant activities of novel synthesized bimetallic boron oxide–zinc oxide nanoparticles. RSC Adv 13(30):20856–20867
38. Parihar V, Raja M, Paulose R (2018) A brief review of structural, electrical and electrochemical properties of zinc oxide nanoparticles. Rev Adv Mater Sci 53(2):119–130
39. Zhang L et al (2007) Investigation into the antibacterial behaviour of suspensions of ZnO nanoparticles (ZnO nanofluids). J Nanopart Res 9:479–489
40. Stankic S et al (2016) Pure and multi metal oxide nanoparticles: synthesis, antibacterial and cytotoxic properties. J Nanobiotechnology 14(1):1–20
41. Colon G, Ward BC, Webster TJ (2006) Increased osteoblast and decreased Staphylococcus epidermidis functions on nanophase ZnO and TiO2. J Biomed Mater Res A: An Official Journal of The Society for Biomaterials, The Japanese Society for Biomaterials, and The Australian Society for Biomaterials and the Korean Society for Biomaterials 78(3):595–604
42. Hashem AH, El-Sayyad GS (2023) Antimicrobial and anticancer activities of biosynthesized bimetallic silver-zinc oxide nanoparticles (Ag-ZnO NPs) using pomegranate peel extract. Biomass Convers Biorefin. https://doi.org/10.1007/s13399-023-04126-8
43. Padmavathy N, Vijayaraghavan R (2008) Enhanced bioactivity of ZnO nanoparticles—an antimicrobial study. Sci Technol Adv Mate 9:3. https://doi.org/10.1088/1468-6996/9/3/035004
44. Gu X et al (2021) Preparation and antibacterial properties of gold nanoparticles: a review. Environ Chem Lett 19:167–187
45. Rosarin FS et al (2013) Antiproliferative effect of silver nanoparticles synthesized using amla on Hep2 cell line. Asian Pac J Trop Med 6(1):1–10
46. Bray F et al (2018) Global cancer statistics 2018: GLOBOCAN estimates of incidence and mortality worldwide for 36 cancers in 185 countries. CA Cancer J Clin 68(6):394–424
47. Verron E et al (2010) Calcium phosphate biomaterials as bone drug delivery systems: a review. Drug Discov Today 15(13-14):547–552
48. Priya MR, K. (2020) and P.R. Iyer, Antiproliferative effects on tumor cells of the synthesized gold nanoparticles against Hep2 liver cancer cell line. Egyptian Liver Journal 10:1–12
49. Zhaleh M et al (2019) In vitro and in vivo evaluation of cytotoxicity, antioxidant, antibacterial, antifungal, and cutaneous wound healing properties of gold nanoparticles produced via a green chemistry synthesis using Gundelia tournefortii L. as a capping and reducing agent. Appl Organomet Chem 33(9):e5015
50. Tahvilian R et al (2019) Green synthesis and chemical characterization of copper nanoparticles using Allium saralicum leaves and assessment of their cytotoxicity, antioxidant, antimicrobial, and cutaneous wound healing properties. Appl Organomet Chem 33(12):e5234
51. Fisher P, Petrini O (1987) Location of fungal endophytes in tissues of Suaeda fruticosa: a preliminary study. Trans Br Mycol Soc 89(2):246–249
52. Hallmann J, Berg G, Schulz B (2006) Isolation procedures for endophytic microorganisms, in Microbial root endophytes. Springer, pp 299–319
53. Suryanarayanan T, Venkatesan G, Murali T (2003) Endophytic fungal communities in leaves of tropical forest trees: diversity and distribution patterns. Curr Sci 85(4):489–493
54. White TJ et al (1990) Amplification and direct sequencing of fungal ribosomal RNA genes for phylogenetics. PCR protocols: a guide to methods and applications 18(1):315–322
55. Altschul SF (1997) Gapped BLAST and PSI-BLAST: a new generation of protein detabase search programs. Nucleic Acids Res 25:3389
56. Abdelghany TM et al (2023) Phytofabrication of zinc oxide nanoparticles with advanced characterization and its antioxidant, anticancer, and antimicrobial activity against pathogenic microorganisms. Biomass Convers Biorefin 13(1):417–430
57. Salem SS (2022) Baker's yeast-mediated silver nanoparticles: characterisation and antimicrobial biogenic tool for suppressing pathogenic microbes. BioNanoScience 12(4):1220–1229

58. Salem SS (2023) A mini review on green nanotechnology and its development in biological effects. Arch Microbiol 205(4):128
59. Vivek R et al (2012) Green biosynthesis of silver nanoparticles from Annona squamosa leaf extract and its in vitro cytotoxic effect on MCF-7 cells. Process Biochem 47(12):2405–2410
60. Elfadel RG et al (2023) Preparation of new surface coating based on modified oil-based polymers blended with ZnO and CuZnO NPs for steel protection. Sci Rep 13(1):7268
61. Mohamed AA et al (2019) Fungal strain impacts the shape, bioactivity and multifunctional properties of green synthesized zinc oxide nanoparticles. Biocatal Agric Biotechnol 19:101103
62. Salem SS, Fouda A (2021) Green synthesis of metallic nanoparticles and their prospective biotechnological applications: an overview. Biol Trace Elem Res 199:344–370
63. Wayne P (2017) Performance Standards for antimicrobial susceptibility testing: twenty-seventh informational supplement M100-S27. Wayne, PA: CLSI
64. Said A et al (2023) Antibacterial activity of green synthesized silver nanoparticles using *Lawsonia inermis* against common pathogens from urinary tract infection. Appl Biochem Biotechnol (In Press). https://doi.org/10.1007/s12010-023-04482-1
65. Ashengroph M, Khaledi A, Bolbanabad EM (2020) Extracellular biosynthesis of cadmium sulphide quantum dot using cell-free extract of Pseudomonas chlororaphis CHR05 and its antibacterial activity. Process Biochem 89:63–70
66. Soliman MK et al (2022) Multifunctional properties of silver and gold nanoparticles synthesis by *Fusarium pseudonygamai*. Biomass Convers Biorefin. https://doi.org/10.1007/s13399-022-03507-9
67. Mohamed AA et al (2021) Eco-friendly mycogenic synthesis of ZnO and CuO nanoparticles for in vitro antibacterial, antibiofilm, and antifungal applications. Biol Trace Elem Res 199:2788–2799
68. Salem SS (2022) Bio-fabrication of selenium nanoparticles using Baker's yeast extract and its antimicrobial efficacy on food borne pathogens. Appl Biochem Biotechnol 194(5):1898–1910
69. Soliman MK et al (2023) Biosynthesis of silver and gold nanoparticles and their efficacy towards antibacterial, antibiofilm, cytotoxicity, and antioxidant activities. Appl Biochem Biotechnol 195(2):1158–1183
70. Brownlee K (1952) Probit analysis: a statistical treatment of the sigmoid response curve. Ann Entomol Soc Am 45(4):686. https://doi.org/10.1093/aesa/45.4.686
71. Sunkar S, Nachiyar V (2013) Endophytes as potential nanofactories. Int J Chem Environ Biol Sci 1:488–491
72. Kumaravel J et al (2021) Mycosynthesis of bimetallic zinc oxide and titanium dioxide nanoparticles for control of Spodoptera frugiperda. Pestic Biochem Physiol 178:104910
73. El-Seedi HR et al (2019) Metal nanoparticles fabricated by green chemistry using natural extracts: biosynthesis, mechanisms, and applications. RSC Adv 9(42):24539–24559
74. Šebesta M et al (2022) Mycosynthesis of metal-containing nanoparticles—fungal metal resistance and mechanisms of synthesis. Int J Mol Sci 23(22):14084
75. Gudikandula K, Vadapally P, Charya MS (2017) Biogenic synthesis of silver nanoparticles from white rot fungi: their characterization and antibacterial studies. OpenNano 2:64–78
76. El-Sayyad GS, Mosallam FM, El-Batal AI (2018) One-pot green synthesis of magnesium oxide nanoparticles using Penicillium chrysogenum melanin pigment and gamma rays with antimicrobial activity against multidrug-resistant microbes. Adv Powder Technol 29(11):2616–2625
77. Qamar SUR, Ahmad JN (2021) Nanoparticles: mechanism of biosynthesis using plant extracts, bacteria, fungi, and their applications. J Mol Liq 334:116040
78. Aldalbahi A et al (2020) Greener synthesis of zinc oxide nanoparticles: characterization and multifaceted applications. Molecules 25(18):4198
79. Kuruppu K et al (2020) Flower shaped ZnO—NPs; phytofabrication, photocatalytic, fluorescence quenching, and photoluminescence activities. Nano Express 1(2):020020
80. Wijesinghe U et al (2021) Biomimetic synthesis, characterization, and evaluation of fluorescence resonance energy transfer, photoluminescence, and photocatalytic activity of zinc oxide nanoparticles. Sustainability 13(4):2004
81. Iranmanesh S, Shahidi Bonjar GH, Baghizadeh A (2020) Study of the biosynthesis of gold nanoparticles by using several saprophytic fungi. SN Applied Sciences 2:1–11
82. Doghish AS et al (2022) Nanocomposite based on gold nanoparticles and carboxymethyl cellulose: synthesis, characterization, antimicrobial, and anticancer activities. J Drug Deliv Sci Techno 77:103874
83. Sui M et al (2019) Strongly confined localized surface plasmon resonance (LSPR) bands of Pt, AgPt, AgAuPt nanoparticles. Sci Rep 9(1):1–14
84. Fouda A et al (2020) Optimization of green biosynthesized visible light active CuO/ZnO nano-photocatalysts for the degradation of organic methylene blue dye. Heliyon 6(9):e04896
85. Munir R et al (2023) Biosynthesis of Leucaena Leucocephala leaf mediated ZnO, CuO, MnO2, and MgO based nano-adsorbents for Reactive Golden Yellow-145 (RY-145) and Direct Red-31 (DR-31) dye removal from textile wastewater to reuse in agricultural purpose. Sep Purif Technol 306:122527
86. Kelly KL et al (2003) The optical properties of metal nanoparticles: the influence of size, shape, and dielectric environment. ACS Publications
87. Prasad KS, Selvaraj K (2014) Biogenic synthesis of selenium nanoparticles and their effect on As (III)-induced toxicity on human lymphocytes. Biol Trace Elem Res 157(3):275–283
88. Elakraa AA et al (2022) Cefotaxime incorporated bimetallic silver-selenium nanoparticles: promising antimicrobial synergism, antibiofilm activity, and bacterial membrane leakage reaction mechanism. RSC Adv 12(41):26603–26619
89. Clarance P et al (2020) Green synthesis and characterization of gold nanoparticles using endophytic fungi Fusarium solani and its in-vitro anticancer and biomedical applications. Saudi J Biol Sci 27(2):706–712
90. Awed AS et al (2019) Unveiling antimicrobial activity of metal iodide (CuI, AgI, and PbI2) nanoparticles: towards biomedical surfaces applications. J Clust Sci
91. Tripathi A, Kumari S, Kumar A (2016) Toxicity evaluation of pH dependent stable Achyranthes aspera herbal gold nanoparticles. Appl Nanosci 6:61–69
92. Almukainzi M et al (2022) Gentiopicroside PLGA nanospheres: fabrication, in vitro characterization, antimicrobial action, and in vivo effect for enhancing wound healing in diabetic rats. Int J Nanomedicine 17:1203–1225. https://doi.org/10.2147/IJN.S358606
93. Soni N, Prakash S (2012) Synthesis of gold nanoparticles by the fungus *Aspergillus niger* and its efficacy against mosquito larvae. Parasitol Res 2:1–7. https://doi.org/10.2147/RIP.S29033
94. Faisal S et al (2021) Green synthesis of zinc oxide (ZnO) nanoparticles using aqueous fruit extracts of Myristica fragrans: their characterizations and biological and environmental applications. ACS Omega 6(14):9709–9722
95. Koutu V et al (2018) Study of the effect of temperature gradient on the thermal and electrical properties of ZnO nanoparticles. in AIP conference proceedings. AIP Publishing
96. Poyraz S et al (2014) One-step synthesis and characterization of polyaniline nanofiber/silver nanoparticle composite

networks as antibacterial agents. ACS Appl Mater Interfaces 6(22):20025–20034
97. Elavazhagan T, Arunachalam KD (2011) Memecylon edule leaf extract mediated green synthesis of silver and gold nanoparticles. Int J Nanomedicine 6:1265–1278. https://doi.org/10.2147/IJN.S18347
98. Fakhari S, Jamzad M, Kabiri Fard H (2019) Green synthesis of zinc oxide nanoparticles: a comparison. Green Chem Lett Rev 12(1):19–24
99. Mishra A et al (2014) Biocatalytic and antimicrobial activities of gold nanoparticles synthesized by Trichoderma sp. Bioresour Technol 166:235–242
100. Davar F, Majedi A, Mirzaei A (2015) Green synthesis of ZnO nanoparticles and its application in the degradation of some dyes. J Am Ceram Soc 98(6):1739–1746
101. Suresh D et al (2015) Green synthesis of multifunctional zinc oxide (ZnO) nanoparticles using Cassia fistula plant extract and their photodegradative, antioxidant and antibacterial activities. Mater Sci Semicond Process 31:446–454
102. Khan SA et al (2018) Green synthesis of ZnO and Cu-doped ZnO nanoparticles from leaf extracts of Abutilon indicum, Clerodendrum infortunatum, Clerodendrum inerme and investigation of their biological and photocatalytic activities. Mater Sci Eng C 82:46–59
103. Castro-Longoria E, Vilchis-Nestor AR, Avalos-Borja M (2011) Biosynthesis of silver, gold and bimetallic nanoparticles using the filamentous fungus Neurospora crassa. Colloids Surf B: Biointerfaces 83(1):42–48
104. Souza TG, Ciminelli VS, Mohallem NDS (2016) A comparison of TEM and DLS methods to characterize size distribution of ceramic nanoparticles. in Journal of physics: conference series. IOP Publishing
105. Meier B (2013) Pressure grows to create drugs for "superbugs.". The New York Times, p 1
106. Shehabeldine AM et al (2023) Potential antimicrobial and antibiofilm properties of copper oxide nanoparticles: time-kill kinetic essay and ultrastructure of pathogenic bacterial cells. Appl Biochem Biotechnol 195(1):467–485
107. Brayner R et al (2006) Toxicological impact studies based on Escherichia coli bacteria in ultrafine ZnO nanoparticles colloidal medium. Nano Lett 6(4):866–870
108. Pal S et al (2018) Synthesis and characterization of ZnO nanoparticles using Moringa oleifera leaf extract: investigation of photocatalytic and antibacterial activity. Int J Nanosci Nanotechnol 14(2):111–119
109. Thakral F et al (2021) Zinc oxide nanoparticles: from biosynthesis, characterization, and optimization to synergistic antibacterial potential. Curr Pharmacol Rep 7:15–25
110. Divyapriya S, Sowmia C, Sasikala S (2014) Synthesis of zinc oxide nanoparticles and antimicrobial activity of Murraya koeiniggi. World J Pharm Pharm Sci (WJPPS) 3(12):1635–1645
111. Al-Dhabaan FA et al (2017) Chemically-produced copper, zinc nanoparticles and chitosan-bimetallic nanocomposites and their antifungal activity against three phytopathogenic fungi. Int J Agric Technol 13(5):753–769
112. Arora N, Thangavelu K, Karanikolos GN (2020) Bimetallic nanoparticles for antimicrobial applications. Front Chem 8:412
113. Ibănescu M et al (2014) Photocatalytic and antimicrobial Ag/ZnO nanocomposites for functionalization of textile fabrics. J Alloys Compd 610:244–249
114. Nagaraju G et al (2017) Electrochemical heavy metal detection, photocatalytic, photoluminescence, biodiesel production and antibacterial activities of Ag–ZnO nanomaterial. Mater Res Bull 94:54–63
115. Wei Y et al (2018) Loose yarn of Ag-ZnO-PAN/ITO hybrid nanofibres: preparation, characterization and antibacterial evaluation. Mater Des 139:153–161
116. Zaheer Z, Albukhari SM (2020) Fabrication of zinc/silver binary nanoparticles, their enhanced microbial and adsorbing properties. Arab J Chem 13(11):7921–7938
117. Dakal TC et al (2016) Mechanistic basis of antimicrobial actions of silver nanoparticles. Front Microbiol 7:1831
118. Abd Elkodous M et al (2020) Fabrication of ultra-pure anisotropic zinc oxide nanoparticles via simple and cost-effective route: implications for UTI and EAC medications. Biol Trace Elem Res 196(1):297–317
119. Low DYS et al (2021) Ultrasound-enhanced biosynthesis of uniform ZnO nanorice using Swietenia macrophylla seed extract and its in vitro anticancer activity. Nanotechnol Rev 10(1):572–585
120. Sanaeimehr Z, Javadi I, Namvar F (2018) Antiangiogenic and antiapoptotic effects of green-synthesized zinc oxide nanoparticles using Sargassum muticum algae extraction. Cancer Nanotechnol 9:1–16
121. Berehu HM et al (2021) Cytotoxic potential of biogenic zinc oxide nanoparticles synthesized from swertia chirayita leaf extract on colorectal cancer cells. Front Bioeng Biotechnol 9:788527
122. Sirelkhatim A et al (2016) Preferential cytotoxicity of ZnO nanoparticle towards cervical cancer cells induced by ROS-mediated apoptosis and cell cycle arrest for cancer therapy. J Nanopart Res 18:1–17
123. Martínez-Torres AC et al (2018) Chitosan gold nanoparticles induce cell death in HeLa and MCF-7 cells through reactive oxygen species production. Int J Nanomedicine 13:3235–3250. https://doi.org/10.2147/IJN.S165289
124. Kajani AA et al (2016) Gold nanoparticles as potent anticancer agent: green synthesis, characterization, and in vitro study. RSC Adv 6(68):63973–63983
125. Wang S et al (2010) Photothermal effects of supramolecularly assembled gold nanoparticles for the targeted treatment of cancer cells. Angew Chem Int Ed 49(22):3777–3781
126. Hamed MM, Abdelftah LS (2019) Biosynthesis of gold nanoparticles using marine Streptomyces griseus isolate (M8) and evaluating its antimicrobial and anticancer activity. Egypt J Aquat Biol Fish 23(1):173–184
127. Lu L et al (2022) Oak gum mediated sustainable synthesis of gold nanoparticles (Au NPs): evaluation of its antioxidant and anti-colon cancer effects. J Exp Nanosci 17(1):377–388
128. Ambujakshi N et al (2019) Chonemorpha grandiflora extract mediated synthesis of Ag-ZnO nanoparticles for its anticancer, electrical and dielectric applications. Materials Research Express 6(9):095068
129. Elsayed KA et al (2022) Fabrication of ZnO-Ag bimetallic nanoparticles by laser ablation for anticancer activity. Alex Eng J 61(2):1449–1457
130. Pandiyan N et al (2019) Ionic liquid - A greener templating agent with Justicia adhatoda plant extract assisted green synthesis of morphologically improved Ag-Au/ZnO nanostructure and it's antibacterial and anticancer activities. J Photochem Photobiol B Biol 198:111559

Publisher's Note Springer Nature remains neutral with regard to jurisdictional claims in published maps and institutional affiliations.